Bulletin of Engineering Geology and the Environment (2021) 80:813–834
https://doi.org/10.1007/s10064-020-01967-9

ORIGINAL PAPER

Landslide-related maintenance issues around mountain road in Dasha River section of Central Cross Island Highway, Taiwan

Meng-Chen Tsao[1] · Wei Lo[1] · Wen-Ling Chen[2] · Tai-Tien Wang[2]

Received: 17 December 2019 / Accepted: 2 September 2020 / Published online: 14 September 2020

Abstract

The winding Dasha River section of the Central Cross Island Highway in Taiwan is 9.44 km long. More than 20% of its length has been rerouted in the past six decades due to landslide-induced maintenance problems. To investigate the influence of geological conditions on the maintenance of this mountainous road section, this study establishes inventories of highway alignments and nearby landslides based on interpretations of multi-temporal aerial photos and highway maintenance records. Types of landslide and topographic features are verified through field investigation, and the engineering characteristics of rock masses are evaluated using the Q-method semi-quantitatively. The results reveal that three sections with rerouting of road or structural modification are located near the undercut slopes of the Dasha River and the boundaries of strata where water erosion and scouring are active and considerable gullies develop. Various metamorphic strata with intricate folds are formed by orogenic deformation and metamorphism under the influence of weathering, such as water erosion and scouring; these evolve into meanders and steep slopes. Gullies develop along the boundaries of strata with distinct lithology, where the engineering characteristics of rock masses vary markedly, disturbing the stability of nearby slopes and hindering the maintenance of the mountain road for long periods. Rerouting the highway and the use of a tunnel instead of the slope-cut-in halfway road effectively mitigate the influence of landslides near meanders where water erosion and scouring are significant. A gallery tunnel effectively mitigates rock fall. However, a gallery tunnel must be constructed without causing overcut-induced slope instability.

Keywords Mountain road · Maintenance · Reroute · Landslide · River erosion · Gully

Introduction

Steep terrain and rapid rivers in mountainous areas lead to unfavorable engineering geological and hydrological conditions for the construction of infrastructures. The cutting of slopes or the filling of roadbeds during the construction of mountainous roads may affect the stability of neighboring slopes (Conforti and Ietto 2019). Even when open to traffic following construction, the roadbeds of a mountainous road often subside unevenly as a result of the scouring of nearby rivers or deep-seated gravitational slope deformations, affecting the track of the road (Wang and Huang 2015; Vuillez et al. 2018; Meneses et al. 2019). Traffic on a mountain road can easily be blocked by rock falls, debris flows, or slope collapses, so the maintaining cost exceeds that of maintaining common highways (Fookes et al. 1985; Calcaterra and Santo 2004; Yang et al. 2012; Camera et al. 2014; Lee et al. 2018b). Despite the low traffic volume on mountain roads, large investments must usually be made in their conservation and maintenance to support social development, land conservation, and disaster prevention and mitigation.

Among the diverse types of landslide (Varnes 1978; Hungr et al. 2014), rock slope movements (rock falls, rock slides, and rock avalanches) are common and they typically cause problems for the maintenance of mountain roads (Mateos et al.

✉ Tai-Tien Wang
ttwang@ntu.edu.tw; taitienwang@gmail.com

Meng-Chen Tsao
niko_cabi_money@hotmail.com

Wei Lo
lowei93@ntut.edu.tw

Wen-Ling Chen
style1224@gmail.com

[1] Institute of Mineral Resources Engineering, National Taipei University of Technology, Taipei, Taiwan

[2] Department of Civil Engineering, National Taiwan University, Taipei, Taiwan

2016; Ragmi et al. 2016). Hungr et al. (1999) investigated rock slope movement-induced risks to two main transportation corridors in southwestern British Columbia using maintenance records spanning four decades. They found that the volumes of 3500 rock movements ranged from less than 1 m^3 to over 4.0×10^7 m^3 and most of the risk to life results from rock falls of intermediate volume 1–10 m^3. Hasegawa et al. (2009) indicated that remnant large-scale landslides are the major causes of debris flows and slides along the major highway passing zones of the Nepalese Himalayas during the monsoon period. Significant hydrothermal alteration and clay mineralization in crushed and jointed rocks have been observed in the failure zones of large-scale landslides, which are related to the faults and folds by active and dynamic geological conditions of the Himalaya Range. Wang (2010) characterized crack patterns on tunnel linings that are associated with shear deformation that is induced by instability of the neighboring slopes. Chiu et al. (2017) reported that the deep-seated gravitational slope deformation induced not only constant road subsidence but also the continuous evolution of lining cracks in a tunnel that passes through a deformed area. Hearn and Shakya (2017) concluded that salient relief, dynamic geology, and heavy rainfall with earthquakes, landslides, floods, erosion, and the formation of sediments accounted for most of the highway hazards in the Himalaya region over the last century.

Slope instability–induced disasters repeatedly affect mountain roads in locations that are close to each other because road sections under unfavorable topographic and geological conditions are fragile. Repair work typically involves restoring passage through damaged sections as quickly as possible, so insufficient time is available to ascertain the factors that affected the disaster or all of the work that is required for complete rehabilitation, leading to repeated disasters (Giordan et al. 2017). Various methods for describing the slope instability–induced risks for mountain roads have been widely discussed in recent years. They include conventional mapping of geological and geotechnical conditions along a road and evaluating the engineering characteristics of rock masses (Siddique et al. 2015; Zheng et al. 2016; Francioni et al. 2019), the use of total station and drone photography to monitor road subsidence and slope displacement (Kovács et al. 2019; Eker et al. 2018), the identification of potential landslides using a high-resolution digital elevation model (DEM) based on airborne or ground-based light detection and ranging (LiDAR) (Breschan et al. 2018; Lee et al. 2018a), analysis of ground displacement using differential interferometry synthetic aperture radar (DInSAR)-related techniques (Bayer et al. 2017; Pappalardo et al. 2018), and the use of data mining models that support statistical regression and probability analyses for the spatially explicit prediction of the susceptibility of a landslide-prone landscape to landslides (Barton et al. 1974; Saha et al. 2005; Bar and Barton 2017; Singh and Kumar 2018; Fallah-Zazuli et al. 2019; Zhang et al. 2019). The relevant literature focuses on evaluation of vulnerable sections in mountain roads, clarifying the factors that influence stability of nearby slopes and developing appropriate maintenance strategies and rehabilitation methods, sometimes as part of a strategy for adapting transport infrastructure to global climate change (Strauch et al. 2015; Palomo 2017; Bordoni et al. 2018; Lentini et al. 2019).

Highway No. 8, Taiwan (referred to as the Tai-8 highway hereafter), was built in the late 1950s mostly by manpower using manual tools. The geological conditions along the route of the Tai-8 highway are complicated, with morphological features that are unfavorable for highway construction, such as cliffs, high and steep slopes, canyons, and erosion gullies. Up to 226 engineering personnel sacrifices were caused by such a difficult construction environment (TPHB 1960). In the six decades since the Tai-8 highway was opened to traffic, more than 250 disasters and road closure events have been caused by landslides, making the Tai-8 highway the highway with the highest disaster potential in Taiwan. The section of Tai-8 highway that winds along the Dasha River has a length of 9.4 km, of which more than 20% has been rerouted because of landslide-induced maintenance problems. This study gathers remote sensing images that have been taken in this area over more than 60 years and records of highway maintenance. The routes of the highway in various periods are examined with reference nearby landslide events. A field investigation is carried out to verify the types of landslide and to semi-quantitatively evaluate rock mass conditions along the route. The effect of the engineering geological conditions on the maintenance and conservation of mountain roads are investigated. Finally, the use of various maintenance strategies to mitigate the influence of slope collapses, gully developments, and river lateral erosion are discussed.

Study area

The Tai-8 highway passes through the Central Range with mostly steep terrain as a result of constant active endogenetic and exogenetic processes in Taiwan. The highway connects western and eastern parts of Taiwan and is also known as the Central Cross Island Highway or the East and West Cross Island Highway. The eastern section of the Tai-8 highway runs through the Liwu River basin, where Taroko, Yanzikou (Swallow Grotto), and Jiuqudong (Tunnel of Nine Turns) are characterized by sheer cliffs and wonderful views. The Liwu River is one of the major rivers in eastern Taiwan and originates between the Hehuan Mountain and the Qilai North Peak with an elevation of more than 3500 m and a length of about 55 km before it flows into the Pacific Ocean. The Liwu River basin is formed from tributaries such as the Shakadang River, the Dasha River, the Waheier River, the Cien River, the Taci

Jili River, and the Sanzhan River; it drains approximately 600 km^2 of steep terrain, which is underlain by metasedimentary rocks. The area has high rates of tectonic uplift in the range 3 to 6 km per million years and high sediment yield, indicating strong forcing and the presence of natural tools for incision of rocks by abrasion (Hartshorn et al. 2002; Liu et al. 2001). Approximately 107 metric tons of sediment moves through the river each year or about 0.1% of the global supply of sediment to the sea (Hartshorn et al. 2002; Milliman and Syvitski 1992). Figure 1 shows the four main sub-basins through which the Tai-8 highway passes before it runs into the canyon section of the Liwu River; the sub-basins are, from upstream to downstream, the Taci Jili River basin, the Cien River basin, the Waheier River basin, and the Dasha River basin.

The Tai-8 highway makes a sharp turn at Sta. 159.5 k near the Houran Pavilion and runs into the Dasha River basin from the Waheier River basin (Fig. 2). The highway heads northward and descends along the right bank of the Dasha River, before turning southward at the Sta. 163.8 k close to the Huitouwan. After it passes through Guyuan and Wenshan, the highway crosses over the Dasha River by the Jhih-huei Bridge at Sta. 168.9 k near Tianxiang where that river converges with the Waheier River to become the Liwu River. The Tai-8 highway meets with the No. 9 highway at Sta. 189.75 k near Taroko after it passes southeast eastward through the canyon of the Liwu River. This study concerns the section of the Tai-8 highway between Sta. 159.5 k and Sta. 168.9 k with a length of approximately 9.4 km (referred to as the Dashaxi section hereafter). The elevation of the Dashaxi section at Sta. 159.5 k near Houran Pavilion is about 1000 m, that at Sta. 163.8 k near Huitouwan is 760 m, and that at Sta. 168.9 k close to Tianxiang is approximately 500 m (Fig. 2a). Topographic limitation by the watershed and confluence point of the Waheier River and Dasha River leads to a 500-m descent along the 9.4-km-long highway section. In this study, the upper road refers to the section between Sta. 161.5 k and Sta. 163.8 k and the lower road refers to the section between Sta. 163.8 k and Sta. 166.0 k; both are winding mountain roads.

Figure 2 b shows a regional geological map of an area that includes the study area (Lo 1992; 1993). Main exposed rock formations in the Dasha River basin include Tianchang Marble, Paiyang Schist, Pilu Formation (composed of phyllite and metamorphosed sandstone and metamorphosed chert), Guyuan Schist, and terrace deposits. The Guyuan

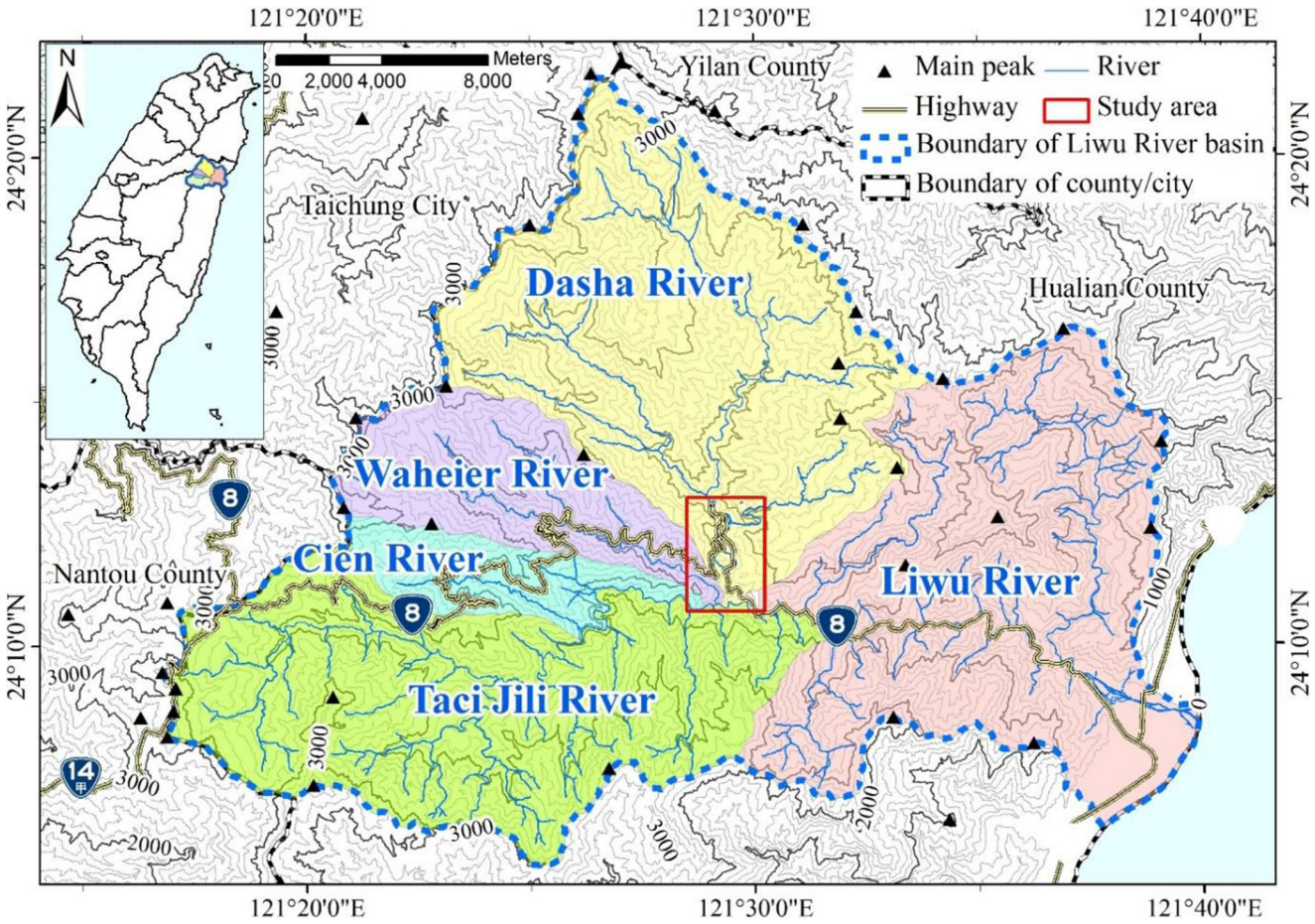

Fig. 1 Liwu River and its five major sub-basins. Study area is marked

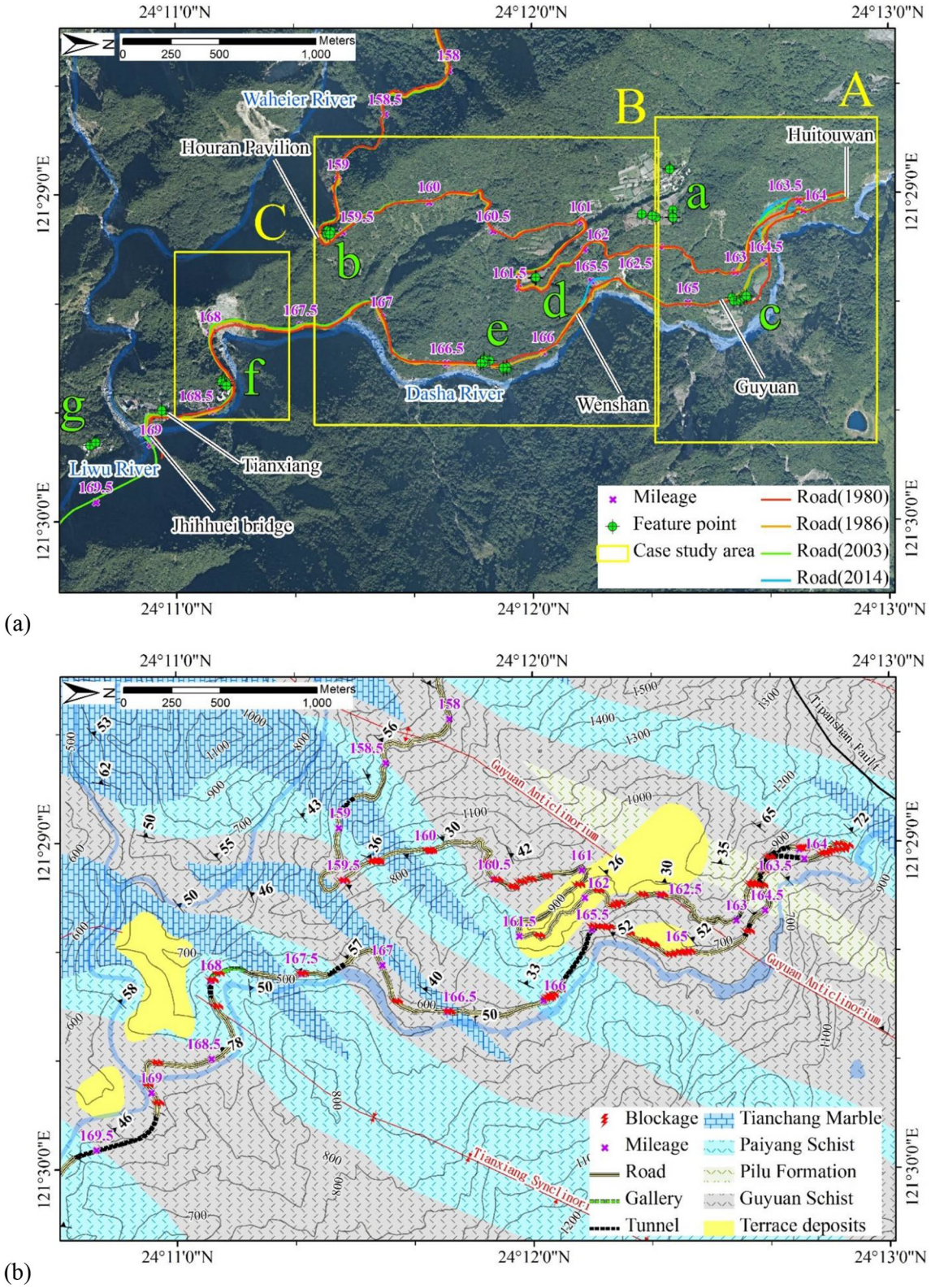

Fig. 2 Route of Tai-8 highway in the study area and regional geology. **a** Three zones in 2014 aerial photograph with locations of feature points used for image processing. **b** Topographic and regional geological map with locations of blockages of highway due to historical disasters

anticlinorium and Tianxiang synclinorium are the major geological structures, and the inferred Tipanshan Fault passes around 0.4 km northwest of Huitouwan. The schistosities of schist formations have strikes in the northeast direction and

typically dip northwest, causing the schistosity generally to intersect the slopes of the upper road and the lower road obliquely or reversely. The Dasha River is winding and narrow, and the water flow is rapid. Some undercut slopes in the attack side of the river are observed to have been formed by vigorous lateral erosion and water scouring, and slip-off slopes are present in the other side. The slopes of the right bank of the Dasha River are mostly in the range 30–60°, increasing to 50–80° in the vicinity of the study section, with local slopes even becoming steep or overhanging as a result of the road construction. Vegetation in the study area is dominated by arbors, and shrubs and herbaceous plants are more developed on the slopes that have recently collapsed. Figure 2 b shows the locations of road disasters and blocking accidents, based on maintenance records since 1990, most of which were induced by slope instability.

Method

Remote sensing images are collected and processed to map the route of the Tai-8 highway, and topographic features and variations are interpreted to investigate the track of some recent landslides and the relationship between the rerouting of the Dashaxi section and the landslides. A field investigation is carried out to verify the records concerning the landslides and to determine the engineering characteristics of the study area, with the purpose of elucidating the causal factors that affect the landslides and the effect of engineering geological characteristics on the maintenance of the mountain roads.

Processing aerial photographs

Figure 3 shows the periods during which collected aerial photographs and images were captured. The 22 photographs and images were taken between 1959 and 2019, covering a time span of 60 years, and are grouped into four classes based on the type of camera used. After 2008, images were taken using a digital camera with a focus length of 120 mm. The camera components and parameters concerning orientation during shooting are provided. Information about the ground control points (GCPs) for photogrammetry is also available. Therefore, a digital surface model (DSM) with high accuracy was produced directly. Photographs were taken during the periods 1997–2008 and 1975–1997 using RMK TOP/TOP2 and RC-10 cameras, respectively, and indicated principal point (IPP), fiducial center (FC), and measure marks (MMs) are available for each photograph. The parameters of exterior orientation, required to produce DSM, were obtained using GCPs, and stereo pairs there were formed by successively shot and partially overlapping photographs. The components of the camera that were used to capture photographs before 1975 were unavailable, so IPP, FC, and MMs could not be obtained, neither the production of DSMs. These photographs were rectified and their locations roughly determined using a limited number of zones with specific features.

To facilitate the analyses of topographic variations and changes in the highway route over the years, all collected aerial photos had to be processed to have the same coordinate system. The TWD97-2010 coordinate system, which is compatible with the World Geodetic System 84, was used, along with local adjustments for the effects of the 1999 Chi-Chi earthquake and the continuous collision of crustal plates near Taiwan. Feature points that exhibit no obvious change are identified within multi-temporal photos and their coordinates in a 2014 image. A field survey that was carried out in 2015 verifies these coordinates in the 2014 image. The shifting, distortion, and deformation of the images are rectified (referred to as "image modification" hereafter) to enhance their spatial accuracy for the subsequent production of the DSM. Figure 4 shows some feature points (Fig. 2a) in multi-temporal photos. For the 1986 image, for example, the root mean squared error (RMSE) of the horizontal coordinates of the 57 feature points is 1.404 m. Points a10, b2, b4, c10, c7, e1, and e2 clearly deviate from their corresponding points in the 2014 image. Image modification produces an average displacement of feature points of 1.788 m, and reduces the RMSE to 1.036 m.

Figure 5 presents the effect of image modification using a traverse net that is formed from some feature points (seven points in Fig. 5a). Figure 5 b to f show the locations of these feature points in the 2014 image (black circles) and their original locations (light blue triangles and light red pentagon) and modified locations (dark blue squares and dark red hexagons)

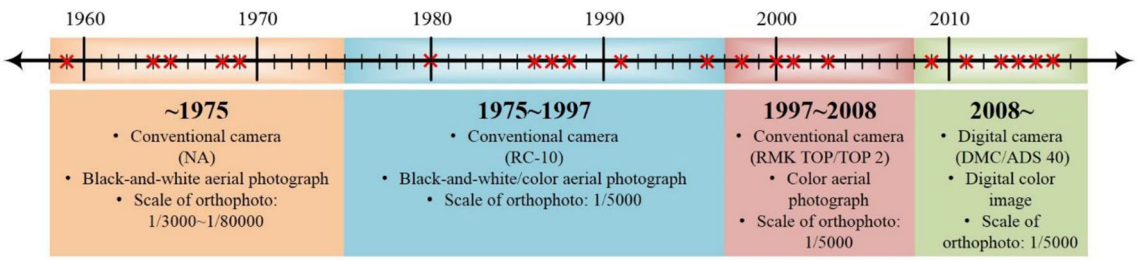

Fig. 3 Collected aerial photographs and images. Four periods are identified according to type of camera used. (Red crosses indicate the year of used photographs)

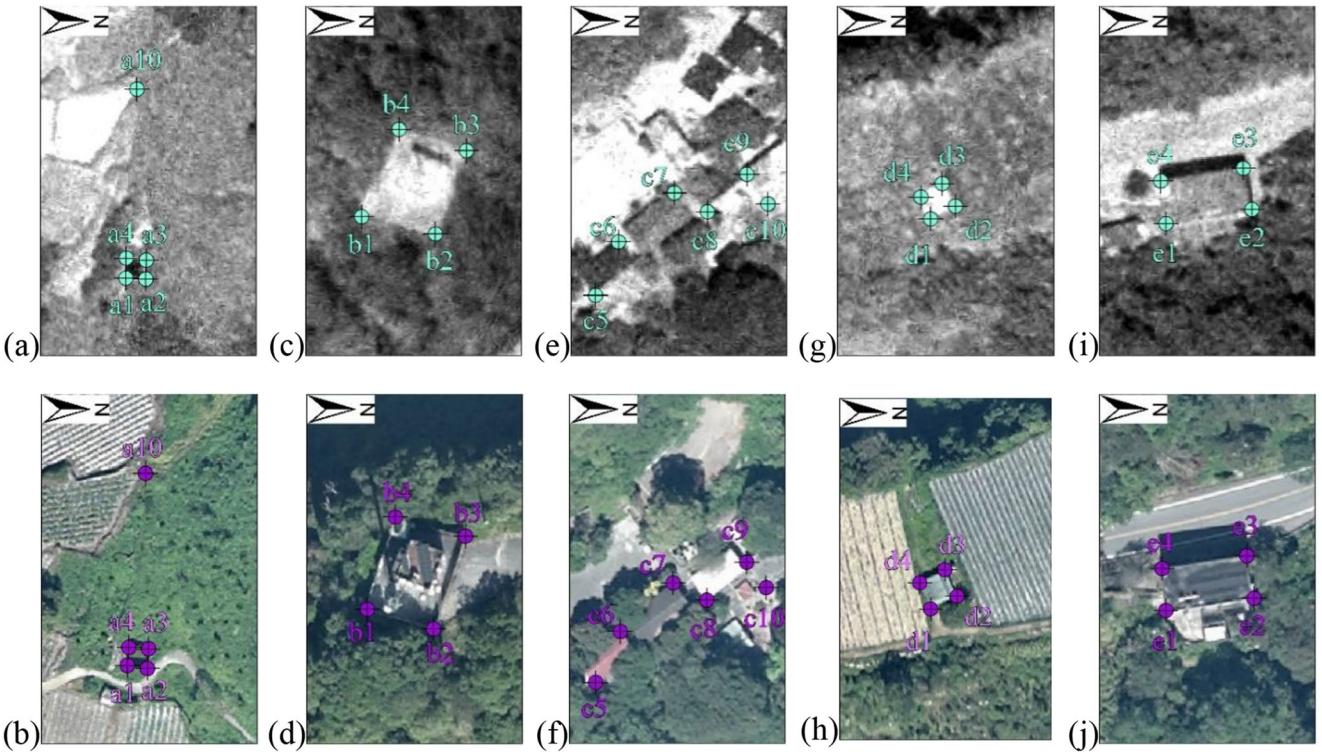

Fig. 4 Feature points in photos taken in different years. **a**, **c**, **e**, **g**, **i** Points a1 to a4, b1 to b4, c5 to c10, d1 to d4, and e1 to e4 in photograph taken in 1986 in that order. **b**, **d**, **f**, **h**, **j** Points in image taken in 2014

in the 1986 photograph and 2001 photograph, respectively. The horizontal shifting of feature points is marked and enlarged. All the feature points in the 1986 and 2001 images had moved toward their corresponding locations in the 2014 image, implying that the used feature points with tiny variations to provide a reference coordinate system effectively overlap the multi-temporal aerial photos in close positions, favoring the interpretation of the landform changes and the production of a DSM for the analysis of topographic variations.

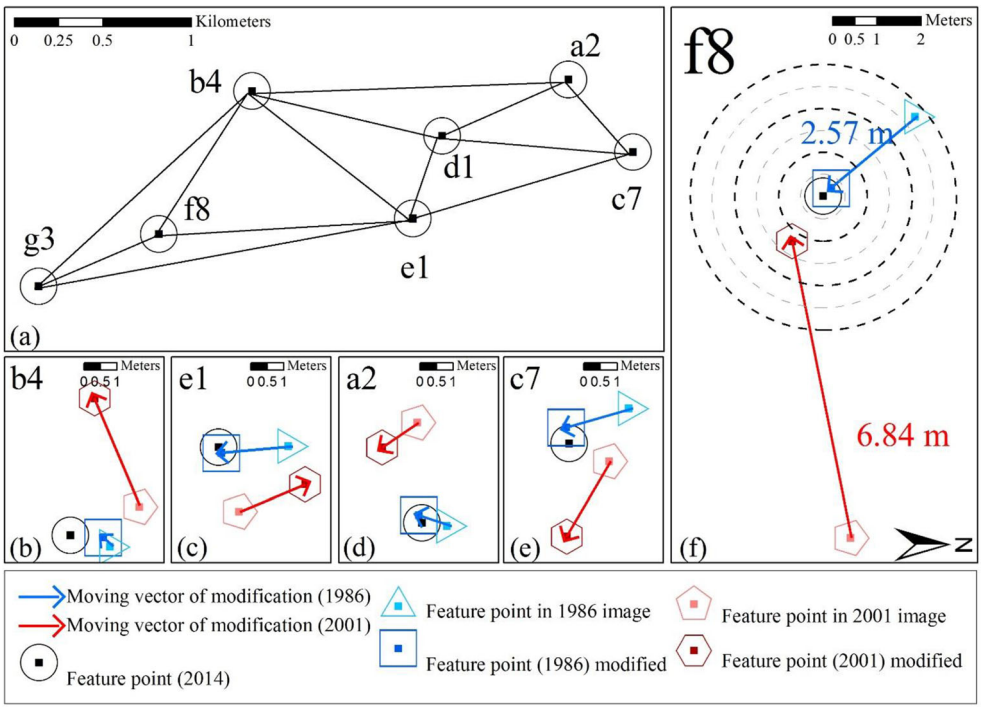

Fig. 5 Traverse net formed by feature points (**a**) and direction and magnitude of displacement of points upon image modification (**b** to **f**). Black circle indicates location of point in 2014 image; light blue triangles and light red pentagon indicate locations of that point in original 1986 and 2001 photos, respectively. Dark blue squares and dark red hexagons indicate locations of corresponding point after image modification, respectively

Figure 6 shows the topographic changes along two profiles upon image modification. The elevations of these profiles are extracted from the DSMs with and without image modification. The elevation of the slope in the 2001 photo is modified, and the average displacement of the feature points (3.625 m) (Table 1) changes the elevations of the upper road and the lower road from those in 2014 DSM, from 5.34 m and 12.07 m to 4.59 m and 10.94 m, respectively (Fig. 6b). However, the modification of the slope is uneven and insignificantly relative to the 1986 profiles. The resolution of the aerial photograph (around 4 m) and the vegetation account for such results. Nevertheless, image modification reduces the differences in the elevations of the upper road and lower road from 4.54 m and 0.94 m to 4.02 m and 0.74 m, respectively (Fig. 6b). Table 1 presents information about the collected aerial photos and RMSEs before and after image modification.

Highway reroute and maintenance records

The highway maintenance branch office has recorded road disasters and blocking accidents since the 1990s. Possible causes of these disasters and accidents are ordinarily described as uphill slope–related damage and roadbed-related damage. Uphill slope–related damage refers to causes of disasters and accidents that are associated with the slope above the road, which include rock fall, slide, avalanche, or even the debris flow. Roadbed-related damage refers to causes that are related to the slope below the road, such as loss of the roadbed; subgrade, subsoil, or natural ground; subsidence, cracking, or displacement of the pavement; sudden depression or bulging along the longitudinal profile of the road; and damage to retaining walls or drainage down the slope from the road, among others. Rock slides, rock avalanches, and headward erosion and lateral erosion of the river bank below the road account for most roadbed-related damage. Based on the maintenance records, of the road disasters and blocking accidents in the studied Dashaxi section, 67% were caused by uphill slope–related damage, 25% by roadbed-related damage, and the remaining 8%, which were road closures, by construction and other factors.

Figure 2 b shows the locations of recorded road disasters and blocking accidents that were caused by uphill slope–related damage and roadbed-related damage. Types of landslide were identified using interpretation of aerial photos and field checks. Since maintenance records before 1990 were lost, highway rerouting and changes in road structures before that time were also interpreted from aerial photos and are marked in figures.

Table 1 RMSE of feature points before and after image modification

Year	Image type	Camera type	Distance before modification (m)	Value of modification (m)	Distance after modification (m)
1959	Aerial photo	–	–	–	–
1964	Aerial photo	–	–	–	–
1965	Aerial photo	–	–	–	–
1968	Aerial photo	–	–	–	–
1969	Aerial photo	–	–	–	–
1980	Aerial photo	RC-10	–	–	–
	Photo base map	–	–	–	–
1986	Aerial photo	RC-10	1.404	1.788	1.036
1987	Aerial photo	RC-10	–	–	–
1988	Aerial photo	RC-10	–	–	–
1991	Aerial photo	RC-10	–	–	–
1996	Aerial photo	RC-10	14.854	13.766	7.041
1998	Aerial photo	RMK TOP	–	–	–
2000	Aerial photo	RMK TOP	–	–	–
2001	Aerial photo	RMK TOP	4.050	3.625	2.520
2003	Aerial photo	RMK TOP 2	–	–	–
	Photo base map	–	–	–	–
2009	Aerial photo	DMC	0.971	0.000	0.971
2011	Orthoimage	–	–	–	–
2013	Aerial photo	DMC	0.88	0.000	0.88
2014	Orthoimage	Referenced period/based on airborne LiDAR			
2015	Aerial photo	DMC	0.56	0.000	0.56
2016	Aerial photo	DMC	–	–	–

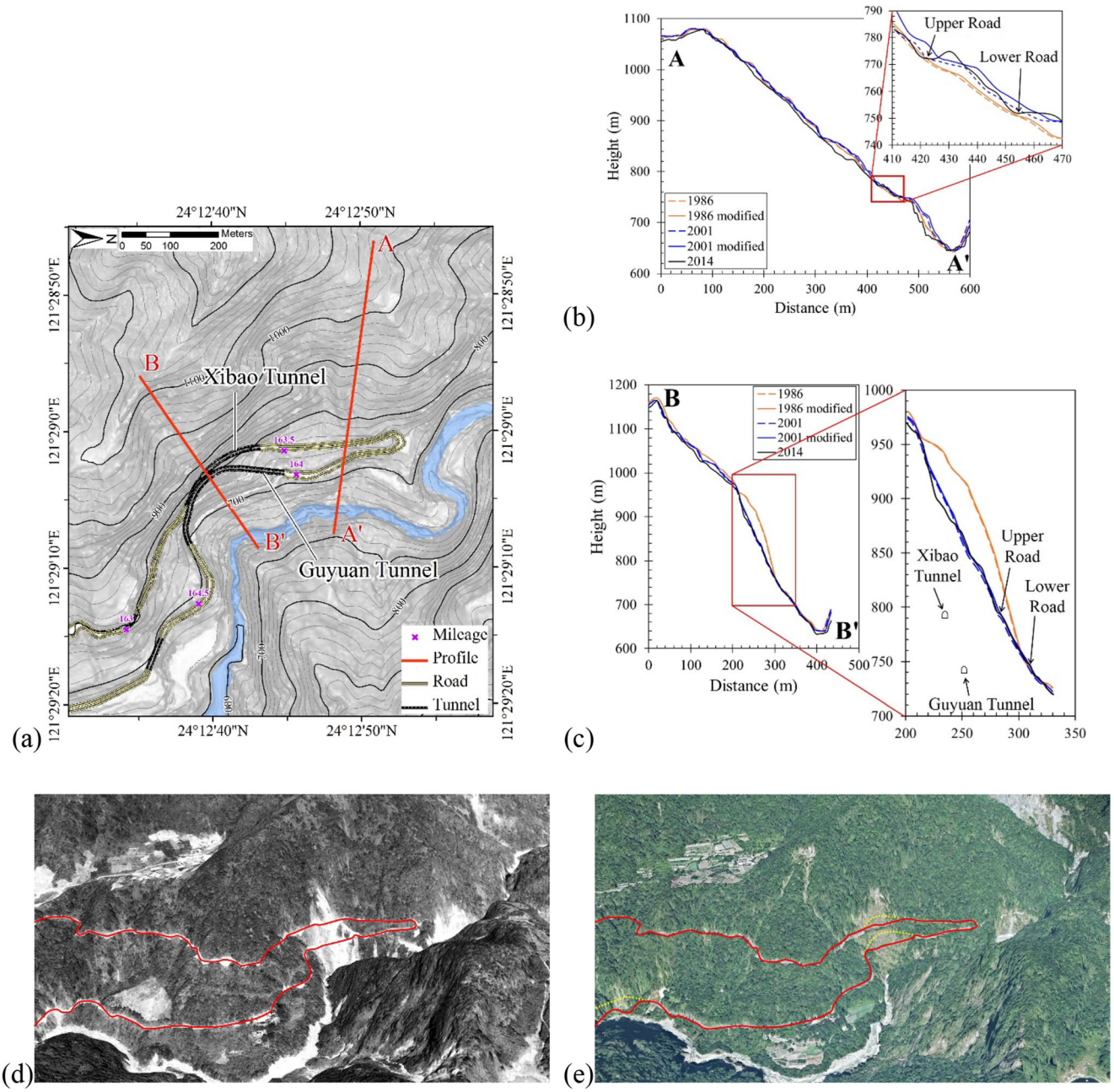

Fig. 6 Locations of two profiles (**a**) and results of image modification (**b** and **c**). Three-dimensional terrain model using aerial photos taken in 1986 (**d**) and 2014 (**e**), after image modification, can be produced within precious location accordingly

Field investigation and rock mass rating

Locations and types of landslide that are interpreted from aerial photos are verified by field investigation, and the records are modified if necessary. Large-scale landslides and major maintenance events, such as highway rerouting and structural change, are identified by interviewing with local residents and engineers who participated in the relevant construction and have retired.

This study adopts the Q-method that was proposed by Barton et al. (1974) for rating the rock mass along the Dashaxi section. In the rock mass rating, an outcrop with a width of approximately 10 m is chosen as the evaluation unit, of which ten segments with similar widths of roughly 1 m are rated separately; the average of the ten results is taken as a representative Q value. If some of the ten segments have very different Q values, the Q-method is applied repeatedly for rating the rock masses in the 10 1-m-wide units to the left and right of those segments, and another one whose middle part involving those segments (Fig. 7). Furthermore, the rating for the water inflow and pressure effects (J_w) and the rating for strength/stress ratio

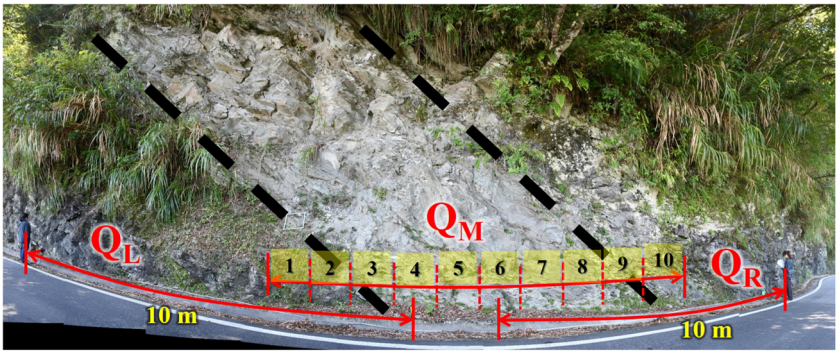

Fig. 7 Outcrop Q value evaluation. Values separately obtained in ten segments at 1-m intervals determine average Q value for outcrop. When Q values in some part of segments are particularly low, values are obtained to the left and right of those segments, and another one whose middle part involved those segments

in hard massive rocks, for faulting, squeezing, or swelling (SRF), have less of an effect on slope stability than during tunneling. Therefore, the ratio J_w/SRF is ignored and set to 1 in this study.

The inferences drawn from the aerial photos are compared with those drawn from the field investigation. The use of Q-method semi-quantitates the mechanical characteristics of rock masses, combined with the interpretation results of multi-temporal aerial photos, and the comparison of the long-term maintenance records of mountain roads, providing valuable information for investigation of the influence of geological conditions on highway maintenance in mountainous areas, and a reference for studying sustainable development maintenance strategy.

Results

Based on the rerouting of the Dashaxi section of the highway, relevant maintenance records, and the locations of landslides interpreted using aerial photos, the study area is divided into three zones to facilitate subsequent discussion. Figure 2 a shows the three zones. The rock mass ratings are obtained using the Q-method. The Q values of 62 evaluation units are in the range 0.14–355.56, with an average of 19.33.

Zone A

Figure 8 shows the highway alignments in zone A of the Dashaxi section over the years. The maintenance history can

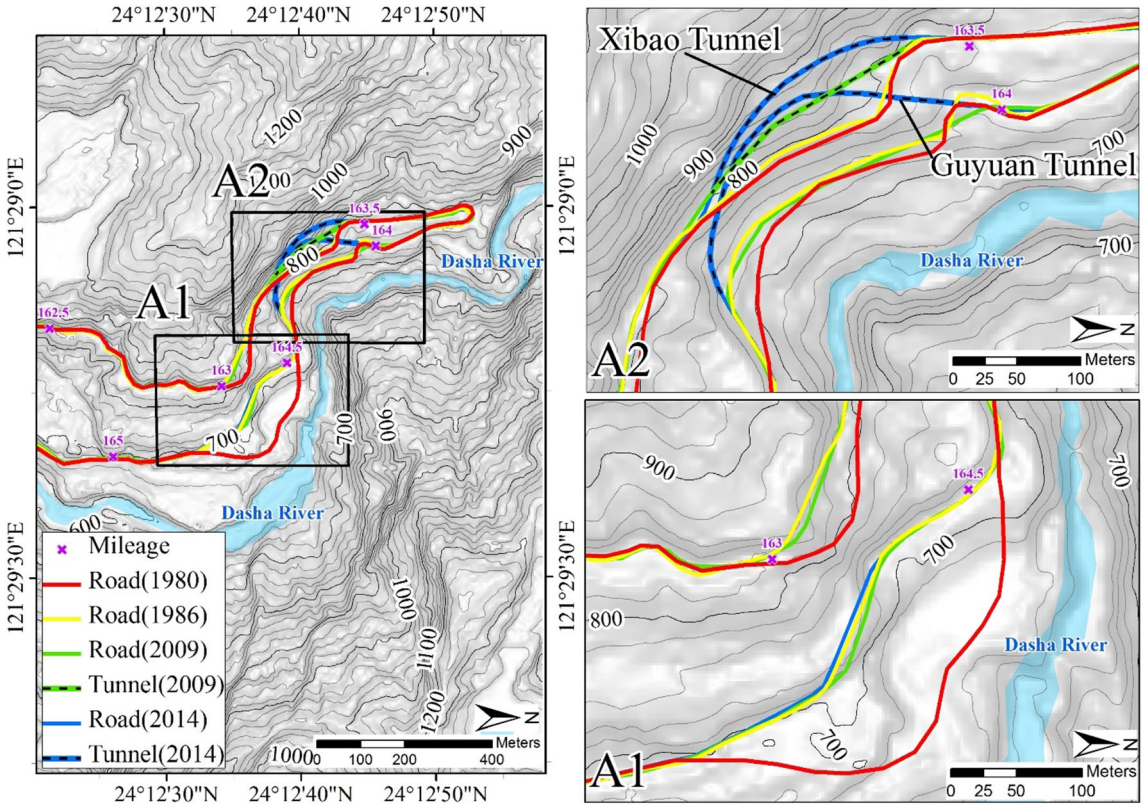

Fig. 8 Highway in zone A of Dashaxi section

be classified into four broad phases based on the highway alignments (Figs. 6 and 8). The first phase started with the completion of the highway and continued until around 1980. During this phase, the highway wound along the contour of the slope and suffered from landslide-related problems. In the second phase, 1980–1986, part of the highway in zone A was substantially rerouted, and the sections near Sta. 163.3 k and Sta. 164.3 k with lengths of 300 m and 350 m, respectively, were moved by about 35 m and 80 m toward the hillside, respectively. During the third phase, 1987–1996, the section in the vicinity of Sta. 163.3 k was further moved toward hillside and the structural type was changed from a slope-cut halfway road to the Xibao Tunnel. Approximately 250 m were rerouted. The fourth phase started in 1996 and has continued to the present; during this phase, the structural type of the section near Sta. 164.2 k was changed from a slope-cut halfway road to the Guyuan Tunnel, and the length of the rerouting was around 350 m. The Xibao Tunnel and Guyuan Tunnel were up to 60 m and 70 m from the original locations of the halfway road, respectively. Some traces of the road sections that were built in the second and third phases are still visible in the aerial photos. Zone A can be split into two subzones. Subzone A1 is located near Guyuan, where the highway was rerouted toward hillside from 1980 to1986 (second phase). The major structure of the highway remains the as-original slope-cut halfway road. Subzone A2 is located to the northwest of A1. The Dashaxi section within the subzone has a large longitudinal gradient. During 1986–1996, the slope-cut halfway road was moved into the neighboring mountain, with critical sections made into tunnels.

The locations of landform change or terrain variation, interpreted from aerial photos, were initially sketched and then preliminarily checked using aerial photos subsequently taken to reduce the probability of misinterpretation. Figure 9 shows the interpreted changes in landform and terrain variation in some years. Aerial photos that were taken in 1959 and 2015 and corresponding interpreted results are also given. Areas with significant landform changes and terrain variations were further sketched, and topographical contours were generated using the 2015 DSM (Fig. 10). Simple codes are assigned for comparison in the figure. The results of the field investigation verify the types of these landslides. The Q values in zone A are in the range 0.26–92.19, with an average of 10.76.

Figure 11 shows the inferred times of landform changes. In the initial stage after completion of the Tai-8 highway, a large proportion of bare slopes was observed and interpreted as shallow slope failures or debris on slopes (Fig. 9a). The slope was cut by blasting without careful consideration of blast holes drilling and charges, and the excavated debris was arbitrarily piled up on the hillside below the road and even dumped down the slopes, affecting the stability of the slope on both sides of the road. In the vicinity of subzone A1, L_A5 was distributed between the upper road and the lower road (Fig. 9b). L_A3, L_A2, and L_A1 were located along the undercut slope of the left curved bank. L_A2 was significant in the 1980 aerial photo (Fig. 9c), which shows debris following the collapse piled up within the Dasha River, causing the river to become narrow to a minimum width of approximately 20 m. Where a slip-off slope had been located, the water flow turned to wash the right bank, causing significant lateral erosion. G_A1 near the boundary between subzones A1 and A2 developed upward from the river side, reaching above the upper road (Fig. 9c). The highway in subzone A1 was rerouted to its current course during 1980–1986 (Fig. 9d). The interpreted L_A4 during the initial stage after completion of the Tai-8 highway was completely exposed. The landslide developed upward above the upper road, with debris piled up to the other side (left bank) of the Dasha River. Several years later, except for the enlargement of L_A2, the slopes in subzone A1 were relatively stable and vegetation recovered. The nearby river was obviously widened in 1996 due to the reactivating of L_A1 and its length and width increased to 400 m and 100 m, respectively (Fig. 9e). Reactivating of L_A1 was observed in the 2000–2003 images. Although the highway was rerouted far from the river and was insignificantly affected by the reactivating of L_A1, the collapsed debris piled up within the river temporally, leading to the development of a new gully (G_A2) from the side of the river. The gully quickly eroded upward, meting G_A1 around 2005 (Fig. 9f–h).

L_A4 and the gullies significantly affected the highway in subzone A2. L_A4 was distributed widely along the highway following its construction, with two gullies north of its (Fig. 9b). Gully G_A1 continuously developed and formed a boundary on the downstream side of L_A4. While L_A4 shrank in downslope side of the lower road, G_A1 developed 10 m above the upper road. The debris of L_A2 piled up in the river and worsened the lateral erosion of the side of the upper stream. L_A4 reactivated in 1986 and became significantly larger (Fig. 9d). The bare slope near L_A4 was steep with debris scattered along the highway. It is believed that the 1986 photo was taken during the highway repair work following the collapse. L_A4 became larger again in 1987, causing the roadbed of the upper road to disappear completely. Around 1987, the upper road was rebuilt in a neighboring mountain, passing through this section in the Xibao Tunnel. Reactivating of L_A4 continued until 1991. During this period, the lower road was rerouted toward hillside and passed through the Guyuan Tunnel. Even after the highway was rerouted, L_A4 was reactivated intermittently. G_A1 met G_A2 in 2005. An opened

Fig. 9 Interpretation of aerial photo for zone A. Aerial photos that were taken in 1959 (**a**) and corresponding interpreted results (**b**). Interpreted results of 1980 photo with contours from orthophoto base map (**c**); results displayed using contours extracted from DSM that is produced using corresponding photos taken in 1986 (**d**), 1996 (**e**), 2009 (**f**), and 2014 (**g**). Aerial photos that were taken in 2015 (**i**) and corresponding interpreted results (**h**) are also given ▶

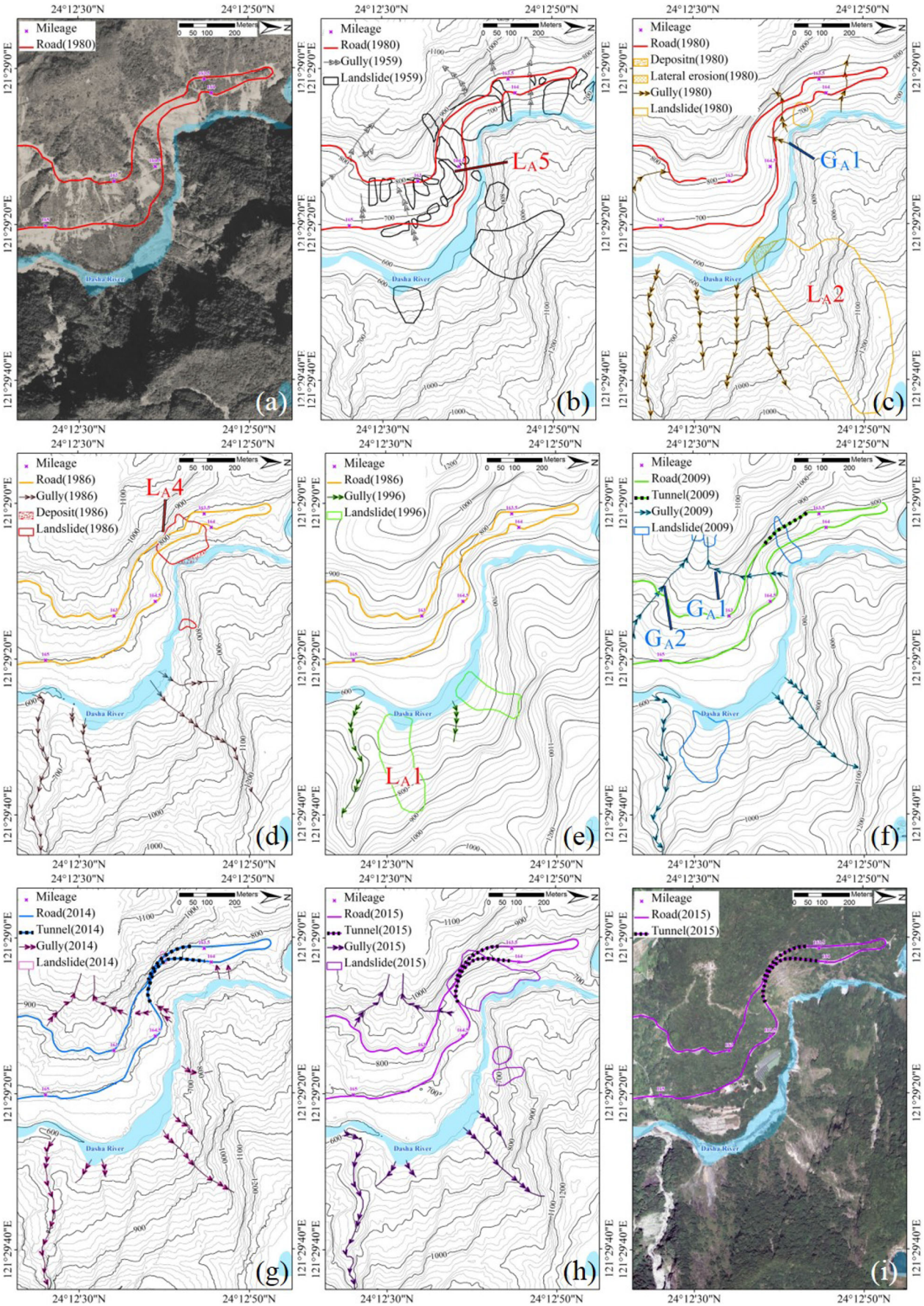
(a)
Mileage
Road(1980)
(b)
Mileage
Road(1980)
Gully(1959)
Landslide(1959)
LA5
(c)
Mileage
Road(1980)
Depositn(1980)
Lateral erosion(1980)
Gully(1980)
Landslide(1980)
GA1
LA2
(d)
Mileage
Road(1986)
Gully(1986)
Deposit(1986)
Landslide(1986)
LA4
(e)
Mileage
Road(1986)
Gully(1996)
Landslide(1996)
LA1
(f)
Mileage
Road(2009)
Tunnel(2009)
Gully(2009)
Landslide(2009)
GA1
GA2
(g)
Mileage
Road(2014)
Tunnel(2014)
Gully(2014)
Landslide(2014)
(h)
Mileage
Road(2015)
Tunnel(2015)
Gully(2015)
Landslide(2015)
(i)
Mileage
Road(2015)
Tunnel(2015)
24°12'30"N
24°12'50"N
121°29'0"E
121°29'20"E
121°29'40"E
Dasha River
Meters
0 50 100 200
N

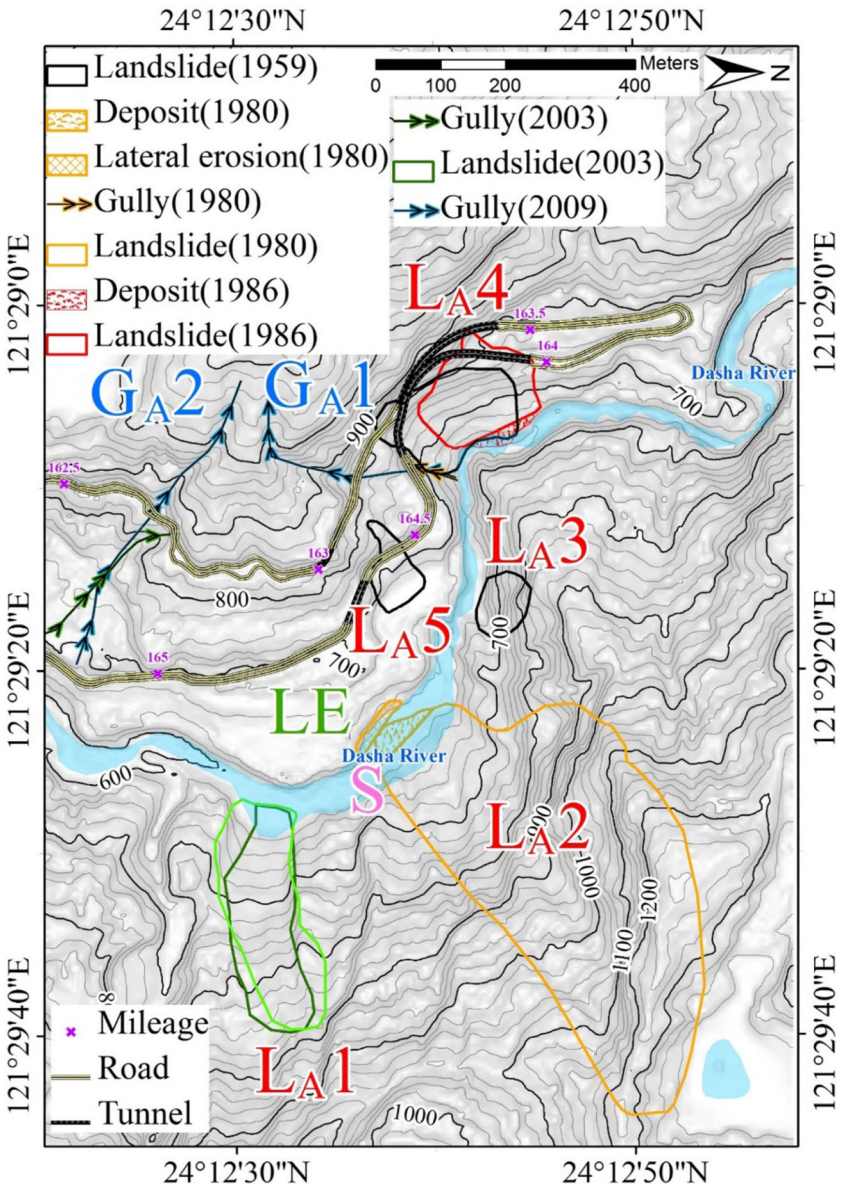

Fig. 10 Variations of terrain in zone A. Contours extracted from DSM, produced using 2015 aerial photo. L denotes landslide, G denotes gully development, LE denotes lateral erosion and undercut slope along a river bank, and S denotes pile-up along a river bank, including a slip-off slope

crack on the vault of the unlined tunnel at Sta. 163 between G_A1 and G_A2 was reported in 2013 (Fig. 12). The recovery of vegetation is observed along G_A2 after mitigation was carried out near the lower road in 2012. However, the scope of bare slope near the area where these gullies met has gradually become larger since then.

Zone B

Figure 13 shows the highway alignments in zone B over the years. Except for the sections between Sta. 165.4 k and Sta. 165.9 k, the highway alignment has varied insignificantly (Fig. 13a). The highway alignment between Sta. 165.4 k and Sta. 165.9 k occurred in three phases in zone B. The first phase started with the completion of the highway and ended around 1964. During this period, the highway wound along slope contours, except for the section between Sta. 165.8 k and Sta. 165.9 k, where an old tunnel with a width of about 4.2 m and a length of around 70 m had been built. This tunnel was rebuilt twice during the second phase, 1964–1993, according to maintenance records. The first rebuilding shifted the section between Sta. 165.7 k and 165.8 k toward the hillside by up to 40 m horizontally, and the slope-cut halfway road section was replaced by a tunnel during 1964–1970. The second rebuilding during 1991–1993 widened the existing tunnel to 7.5 m and rerouted the highway northwest of the tunnel into the current Taishan Tunnel with a length of 304 m. The maximum horizontal movement was 45 m. The third phase of highway alignment continues from 1993 to the present. The alignment remains similar to that at the end of the second phase, except that some parts were widened or modified to increase the horizontal curvature enlargement along the original course.

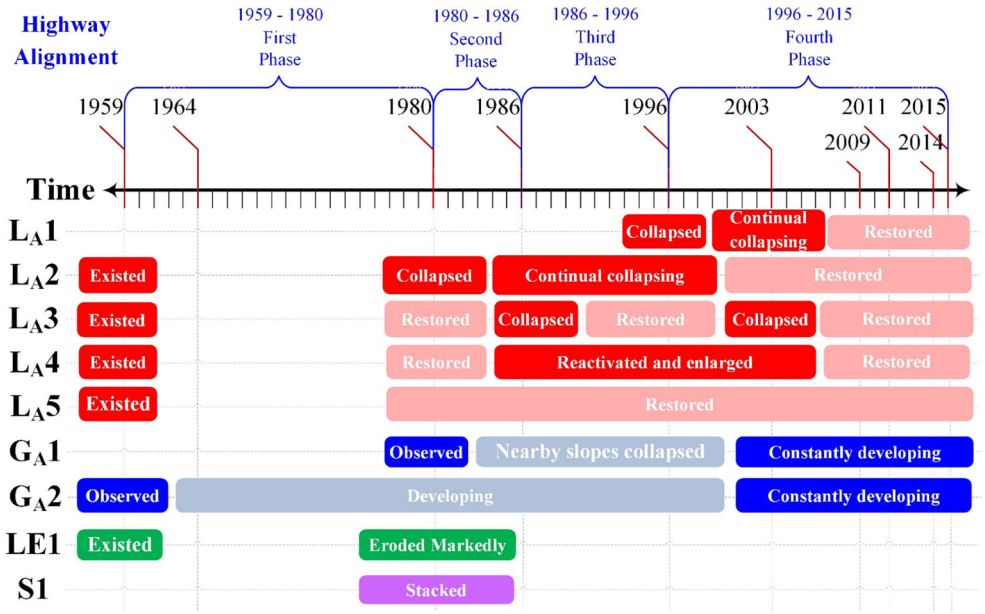

Fig. 11 Diachronic variation of interpreted landslides and gullies in zone A

The gully is the most significant morphological features that are observed in aerial photos. In the first stage after completion of the highway, six gullies, G_B1 to G_B6, were present between the side of the Dasha River and the upper road (Fig. 13b, c). G_B2 and G_B3 developed southwestward from the sharp turning point of the Dasha River near Sta. 165.6 k of the Tai-8 Highway, and the other four gullies developed northwestward and were approximately perpendicular to the boundary of the strata in the study area. In Fig. 13 b, the slope in the vicinity of the intersection of highway in the first phase with G_B3 and the original tunnel is high and almost overhangs to form cliff, and frequent rock falls have been reported. The modification of this section into a tunnel was once suggested following the completion of the Tai-8 highway (Lee 2011). The aerial photos show frequent collapses close to the intersections of the highway with G_B2 and G_B3, among which the landslide L_B2 was insignificant in 1986 and appeared only in the slope toe near the right bank of the Dasha River in 1987. L_B2 was larger in the next six aerial photos (1988–2001), resulting in the rerouting of the nearby slope-cut halfway road into a tunnel in the neighboring mountain. Landslide L_B1 was observed after the completion of the highway but was not visible from 1980 to 2013, because of the recovery of vegetation. The reactivating of L_B1 was detected near the bottom of gully G_B1, and a corresponding countermeasure was performed in 2015.

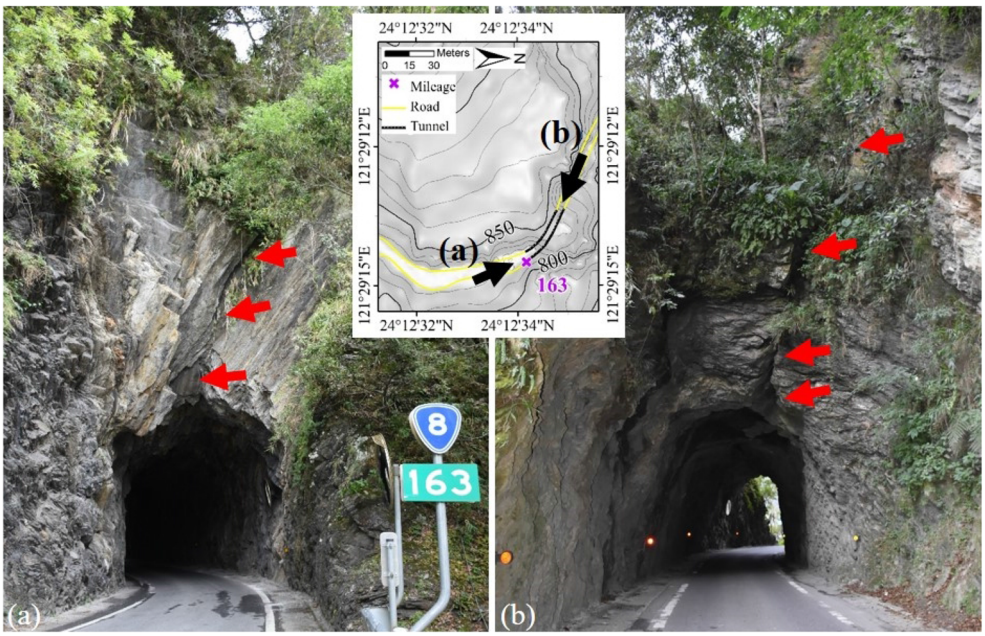

Fig. 12 Images of unlined tunnel near Sta. 163 k. Opened fracture observed on tunnel vault (**a**) and developed to slope surface above tunnel (**b**)

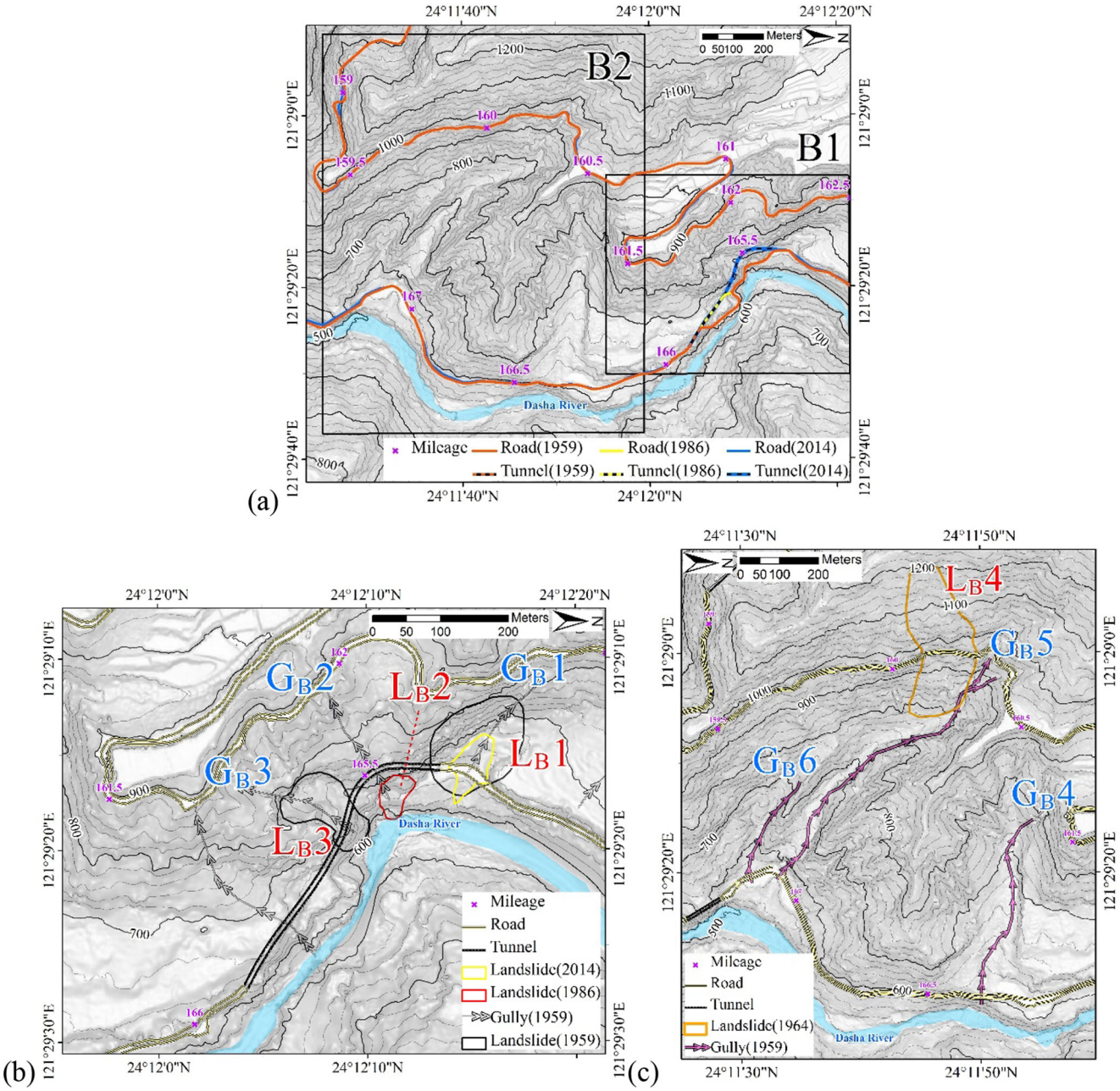

Fig. 13 Variations of highway alignment in zone B (**a**). Topographic feature varied in subzones B1 (**b**) and B2 (**c**)

In Fig. 13 c, G_B4 to G_B6 are markedly longer than G_B1 to G_B3. Collapses are identified on the slopes along both sides of G_B4 to G_B6 in successive aerial photos. The spatial distributions of these collapses are typically northeast-southwest. Landslide L_B4, which occurred in the head area of G_B5 in 1964, is representative. Since mitigation measures were taken in response to L_B4, its activity was far less than that of L_B2 and the slope near L_B4 has been stable for more than five decades. In contrast, in the vicinity of the intersection of G_B4 with the Dasha River, the river bank has gradually shrunk over a long period and has exhibited features of potential collapse in recent aerial photos. Figure 14 shows the diachronic variation of interpreted landslides and gullies in zone B. The Q values in zone B are in the range 2.38–25.10, with an average of 7.05.

Zone C

Figure 15 shows the highway alignments in zone C. The alignment of the Tai-8 highway as built in the 1960s had not changed, and the road winds along the slope contours, but the width of the highway and its structural type in some sections have changed. Figure 15 b plots the profile near Sta. 167.8 k, where the Dasha River flows southward, making a short turn to flow northeast-eastward. Highway maintenance is divided

into three phases, with different widths and structures. In the first phase following the completion of the highway to 1986, the road was mostly 5–6 m wide. The Tianxiang Tunnel near Sta. 167.8 k, almost perpendicular to the Tai-8 highway, was built in 1986. The Tai-8 highway in the vicinity of Sta. 167.8 k was then widened to approximately 8 m. The second phase started in 1986, when the hillside slope of the highway was cut to further widen the road to over 10 m, and limited slope protection measures were used for the excavation. In 2001, gallery tunnel with a length of around 180 m was built close to the sharp turning point of the Dasha River. The gallery tunnel was designed using a conventional method with a foundation depth of 1.5–2.0 m. The hillside slope had to be cut to build the foundation (the enlarged view of Fig. 15b). This gallery tunnel was damaged in Sep. 2008 by collapse of the slope (Fig. 16a). Repairing work was promptly carried out at the end of 2008. However, more than 40 m of the gallery tunnel was destroyed by another severe slope in Oct. 2009 (Fig. 16b). The tunnel was reconstructed and extended to 270 m, which is its length today. After the reconstruction work had been completed, highway maintenance entered the third phase, which continues to today.

Gully G_C1 is visible in the aerial photo before highway construction and was larger immediately after completion of highway but could not be seen in 1986 since the recovery of vegetation. The bare slope near the construction site of Tianxiang Tunnel at Sta. 167.8 k, visible in 1986, was invisible in the 1988 photo. Landslide L_C2 could be seen in 1991 because of the nearby construction of a parking area at the riverside. Local drainages were modified accordingly, causing the lower part of gully G_C2 to be gradually shifted from the northern boundary of L_C2 southward to its middle area. The highway in zone C was widened in 1996 by cutting into the hillside slope. Local collapses can be seen near the cut slope in the 1998 photo. The collapse near G_C1, which developed upward, was significant, reaching the local hill ridge in 2000. In the 2001 aerial photo, the gallery tunnel was wider than the highway. The hillside slope in the gallery tunnel had been cut to maintain the width of the road and to enable the construction of the gallery foundation. The bare slope along G_C1 was enlarged and interpreted as landslide L_C1 or the reactivating of piled debris along G_C1. L_C1 was larger in 2003 and again in 2009. Meanwhile, two new gullies developed from the middle part of the slope and two landslides (L_C1A and L_C1B) were observed; gullies G_C3 and G_C4 developed upward to their corresponding upper cliffs. The landslide in Oct. 2009 was large and merged with L_C3, L_C4, and their neighboring area to form the huge L_C5. Mitigation measures were completed at the end of 2012. However, new bare slopes above the gallery tunnel and close to the hill ridge are observed in the 2019 image, in which debris was scattered in G_C2 and had moved downward. Figure 17 shows the diachronic variation of interpreted landslides and gullies in zone C. The Q values in zone C are in the range 0.14–355.56, with an average of 21.98.

Discussion

The rerouted sections of the highway in subzones A1 and B1 and the section with the modified structure in zone C are all neighbored to the undercut slopes along the meanders of the Dasha River. Gullies had developed upward from the river

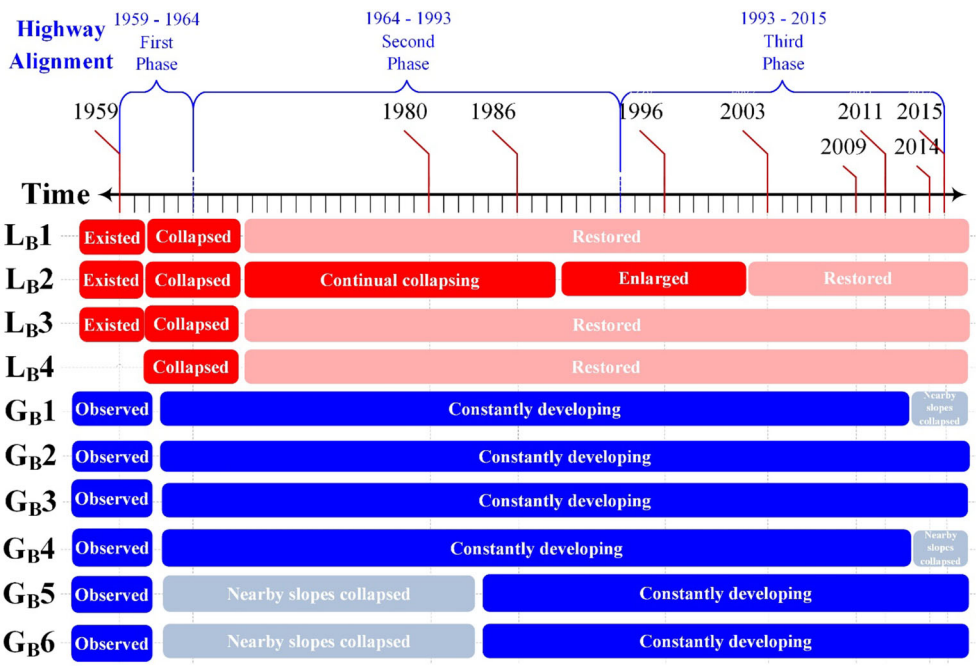

Fig. 14 Diachronic variation of interpreted landslides and gullies in zone B

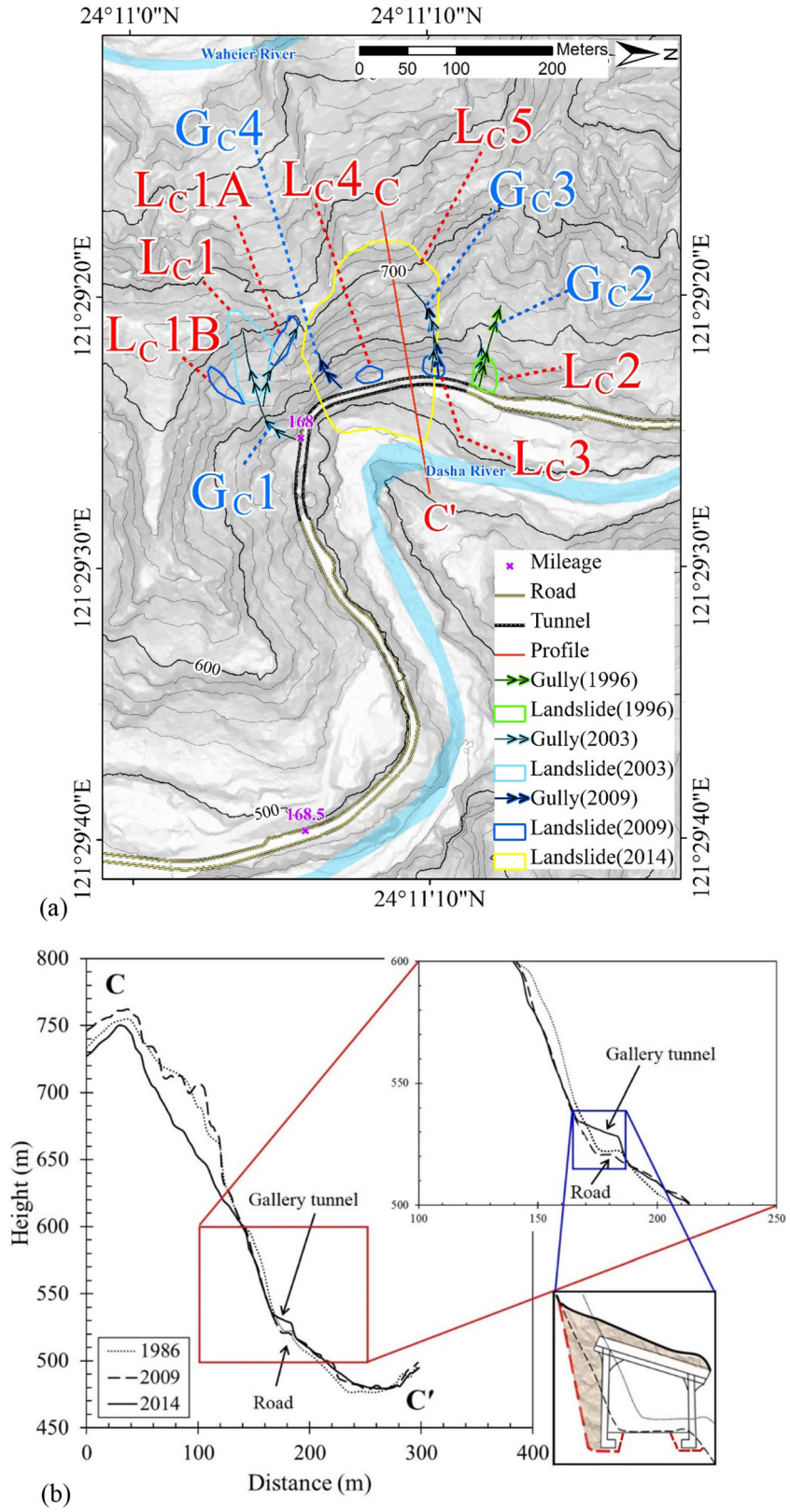

Fig. 15 Variations of terrain in zone C (**a**) and profile of EE' (**b**)

bank before the construction of the Tai-8 highway. After the completion of the highway, slopes frequently collapsed close to the gullies that had developed near the undercut slopes of the Dasha River. Obviously, the rerouting and changing of the structure of the Dashaxi section of the highway related to neighboring slope collapses, which were further influenced

Fig. 16 Gallery tunnel successively damaged in Sep. 2008 (**a**) and Oct. 2009 (**b**)

by the development of gullies and erosion by flowing water in the meanders of the Dasha River.

The rerouted section toward hillside in subzone A2 locates in the slip-off slope of the Dasha River, that is different from the aforementioned subzones of the neighboring undercut slopes. The landslide in the upper slope of this section was not significant. The highway was rerouted in this subzone because of the loss of its lower slope as a result of bank erosion that occurred when the direction of water flow was changed by the mass of debris in the river. This debris was associated with the large landslide on the opposite side of the Dasha River in the 1960s, where an undercut slope was also present. Riverside undercut slopes in the study area clearly affect the stability of their hillside slopes by lateral erosion of water flow and the development of accelerating gullies. When a landslide is large enough to leave debris in the river that will also change the direction of water flow.

The gullies were distributed mostly in the northeast-southwest direction and, subsequently, in the northwest-southeast direction. The northeast-southwest gullies typically develop along various lithological boundaries and are short, steep, and densely distributed. Turowski et al. (2008) indicated that in addition to the regional anticlinoria and synclinoria, river erosion and the variability of flow influence the development of gullies. In contrast, the northwest-southeast gullies are relatively long and gentle. G_B5 and G_B6 are representative of the northwest-southeast gullies, which are thought to be associated with the fractural structures that are perpendicular to the regional anticlinoria and synclinoria (Lo 1992).

The effects of river erosion and scouring on slope stability are determining by examining the collapses in the vicinity of G_B2 and G_B5. G_B2 is close to an undercut slope of the Dasha River. Successive collapses near the G_B2, visible in the multi-temporal aerial photos, typically had moderate scales. However, such collapses inhibited the maintenance of the slope-cut halfway road until the highway was rerouted toward hillside and through the Taishan Tunnel. The meander where G_B5 intersects with the Dasha River had a large radius and was wide, with relatively little bank erosion, and insignificantly affected the development of G_B5. The slope close to the head area of G_B5 slid more than 100 m wide and 200 m long in the 1960s. However, it has been stable for more than five decades after mitigation. Obviously, the stability of the slopes near the head areas of the gullies in the study area can be maintained for a relatively long time when an exogenic force acting on the gully, for example the river erosion and scouring, is not significant. Strong erosion and scouring of the river bank account for the fact that the development of the northeast-southwest gully G_A1 in the subzone A2 is much faster than that of the northwest-southeast gully G_A2. Accordingly, the mitigation measures associated with G_A2 were only carried out in its lower part, effectively slowing the head-ward development of G_A2 in the past 7 years.

The distribution of the Q values of rock masses along the Dashaxi section provides further information about factors that may affect the development of gullies and landslides. The Q values along the highway in the study area are in the range 0.14–355.56 representing a variation of about 2540 times. However, the Q values near both sides of the gullies or lithological boundaries are interesting. Figure 18 a shows the lithology that is exposed along the highway between Sta. 159.4 k and Sta. 160.2 k and the obtained Q values. Figure 18 b shows the distribution of Q values perpendicular to the boundaries of strata: the first, second, and third quantiles of the ten Q values for each outcrop, based on an interval of about 1 m, are plotted. The Q values that are obtained in a stratum are mutually inconsistent, and the ten Q values for each outcrop vary much more. Such variations are most significant in the vicinity of strata boundaries or even the boundaries between various lithologies in a stratum. Figure 7 shows a representative result of Q-method from an outcrop near a boundary of strata. The average Q values of the rock masses to the left and right of the boundary are 85.28 and 46.73, respectively. However, the Q values of the 6 units involving the boundary are in the range 0.35–3.42, with an average of 1.20. Among the six rated items of the Q-method, the rated

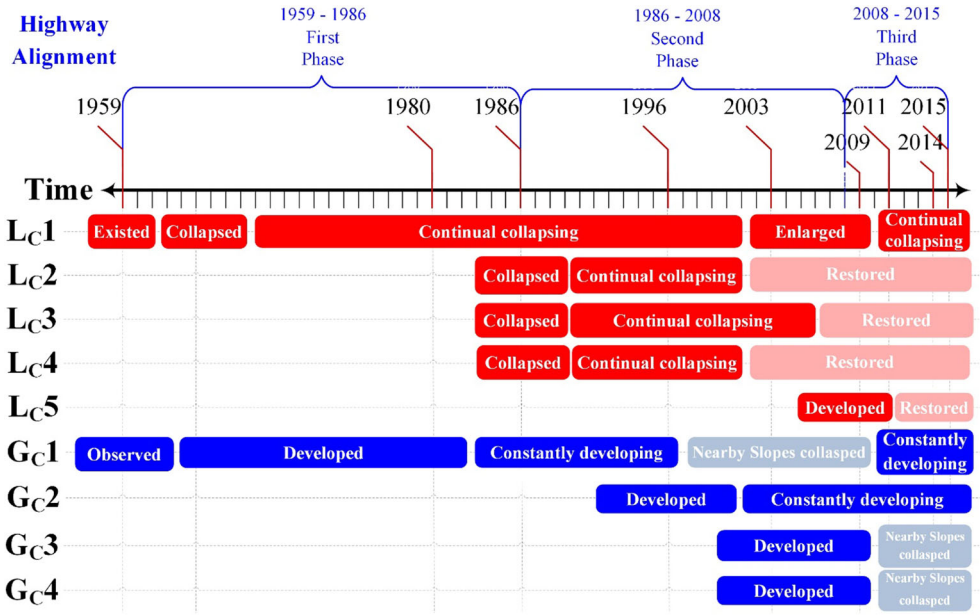

Fig. 17 Diachronic variation of interpreted landslides and gullies in zone C

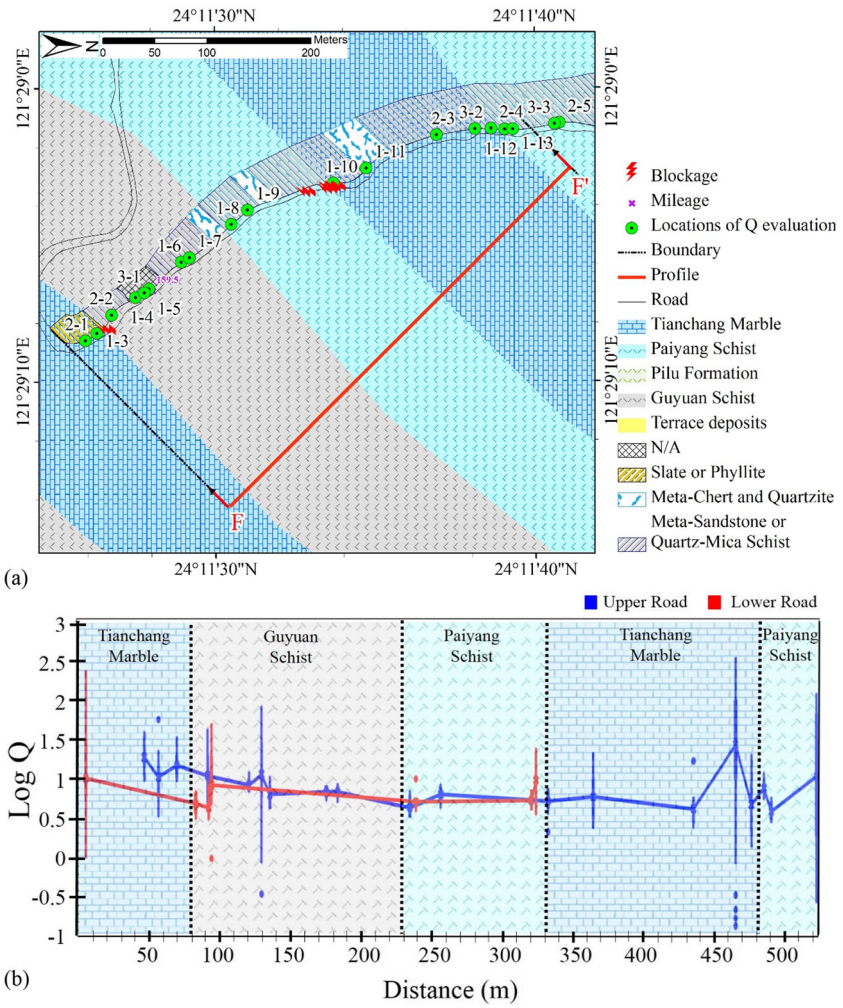

Fig. 18 Locations where Q values are obtained between Sta. 159.4 k and Sta. 160.2 k (**a**) and obtained Q values of rock masses (**b**)

results for RQD and J_n vary obviously near the lithological boundaries.

Figure 19 b plots the variation of Q values in different strata along the direction that are perpendicular to the strata boundaries (Fig. 19a). The Q values of the rock masses in the upper road are typically greater than those in the lower road. Again, the Q values which vary significantly are generally close to the boundaries of strata or lithological boundaries in a stratum. Among the four major strata that were exposed in this study, Tianchang Marble has the highest Q values, in the range 0.14–355.56, with an average of 30.52. The Q values of Paiyang Schist, Pilu Formation, and Guyuan Schist are in the ranges 0.27–124.14, 0.26–92.19, and 2.29–16.67, respectively, with their respective averages of 17.64, 13.06, and 6.38 (Fig. 19c, d). The Q value that is evaluated using an interval of 1 m can be as low as 0.14 close to the boundary between Tianchang Marble and Paiyang Schist. The Tianchang Marble stratum exhibits the greatest variation in Q values. The Q values close to the section Sta. 166.5 k are lower than those in the vicinity of Sta. 159.4 k, Sta. 159.8 k, and Sta. 167.7 k (all marked in

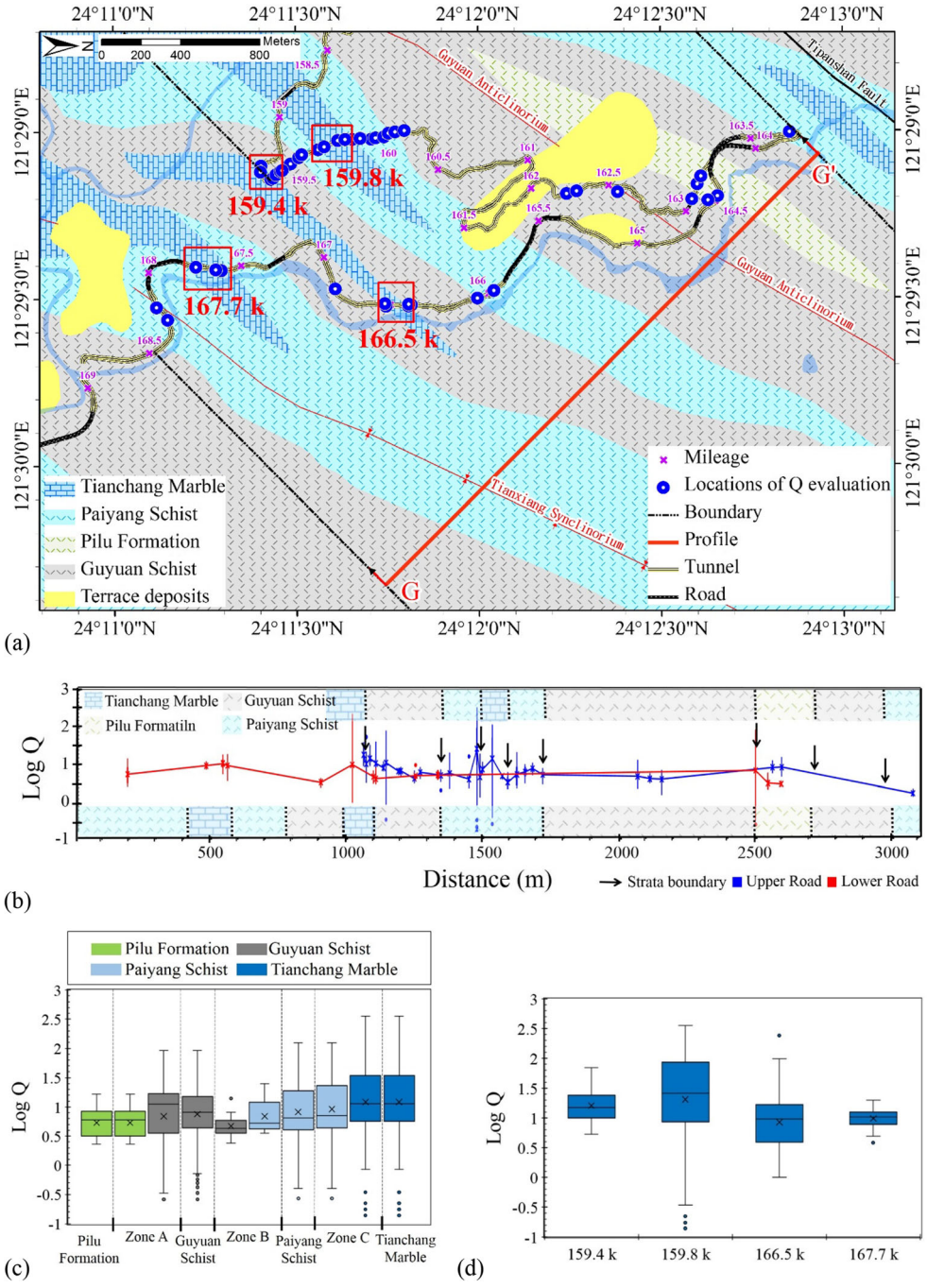

Fig. 19 Locations where Q values are evaluated in the study area (**a**) and obtained Q values of rock masses (**b**). Q values of rock in various strata (**c**) and at various locations in Tianchang Marble (**d**)

Fig. 19a). The rock masses in the lower road were significantly affected by river erosion and scouring, and the Tianchang Marble was relatively thin near Sta. 166.5 k, making the rock masses of the Marble vulnerable to fracture under strong tectonic folding, accounting for the lower Q values in this section. Additionally, the average Q values near the axes of the Guyuan anticlinorium and the Tianxiang synclinorium are low, and those evaluated using 1-m intervals vary negligibly. With the exception of the L_A2 in subzone A2 near the axis of the Guyuan anticlinorium, few landsides were observed near the axes of the anticlinorium and synclinorium. The impact of geological folds on landslides is not as significant as that of river erosion, scouring, or gully development.

Various metamorphic rocks in the study area have been deformed into a number of open, asymmetrical, or overturned folds and intricate flow folds as a result of multiple phases of orogenic deformation and metamorphism. The studied section of the Tai-8 highway which winds around the slope of the right bank of the Dasha River is downgraded and crosses the axes of the Guyuan anticlinorium and Tianxiang synclinorium. The strikes of the strata and the cleavage of the lithology are typically northeast-southwest and close to the plunge of the fold axes. The strata have various lithologies with different competences of rocks, and they sustain a wide range of degrees of deformation under tectonic and regional geological activities, causing the rock that is exposed in the slope to exhibit fractures with various appearances. The geometric characteristics of the fractures, such as their spacing, persistency, and roughness, vary substantially. Therefore, the rating of RQD and J_n for the Q-method is low on the boundaries among the strata or the lithological boundaries in a stratum. The Dasha River causes erosion and scouring, deteriorates nearby rock formations associated with other factors, and forms steep slopes along its bank. Cut slopes are inevitably formed in the construction of a mountain road and are protected using artificial countermeasures, which may suffice in the short term to mitigate landslides as a result of rainfall, earthquakes, and water scouring. After many years, sections with unfavorable engineering characteristics fail to withstand long-term river erosion, scouring, and gully development. Rerouting the highway toward the hillside and modifying is structural type from a slope-cut halfway road to a tunnel to reduce the effects of these strong exogenic forces are effective in the study area, according to the few maintenance records from the last two decades. A gallery tunnel is effective for mitigating rock fall from a hillslope of a highway. The overcutting of a roadside slope should be avoided during the construction of a gallery tunnel to prevent artificial excavation-induced instability.

Conclusion

This study concerns the section of the Tai-8 highway that winds along the right bank slope of the Dasha River, and establishes inventories of highway alignments and nearby landslides from multi-temporal aerial photo and highway maintenance records. Types of landslide and topographic features are verified by field investigations, and the engineering characteristics of rock masses that are exposed on outcrops along the highway are evaluated using the Q-method semi-quantitatively. The effects of engineering geological conditions on the maintenance and conservations of mountain roads, and the related effectiveness of maintenance strategies in mitigating neighboring slope collapses, gully development, and river erosion and scouring, are investigated. The following conclusions are drawn:

1. Multi-temporal aerial photos and highway maintenance records indicate that, following the completion of the 9.4-km-long Dashaxi section of the Tai-8 highway in 1960, three sections with a total length of about 1.9 km were rerouted or their structural types were modified. These three sections are all close to the undercut slopes of the Dasha River, and the boundaries among strata where water erosion and scouring are active and gullies develop strongly.
2. The Q values of rock masses in the lower road are typically less than those in the upper road. The Q values near the boundaries of the Tianchang Marble, Paiyang Schist, Pilu Formation, and Guyuan Schist strata and those of the lithological boundaries in each stratum are generally small. In addition, rock mass with a low Q value is observed in the thin section of competent Tianchang Marble that is interbedded in relatively incompetent Guyuan Schist.
3. The aforementioned strata have various lithologies with different competences of rocks and sustain a wide range of degrees of deformation under tectonic and regional geological activities. The differential erosion that is caused by the various competences of the strata generates meanders in the Dasha River with steep slopes. Rock masses in the vicinity of strata boundaries and lithological boundaries in each stratum have a large range of Q values, corresponding to a large variation in their engineering characteristics. The cut slope and associated protection measures suffice in the short term to maintain stability under the effects of rainfall, earthquakes, and water erosion and scouring. However, after many years, the sections with unfavorable engineering characteristics eventually fail to withstand river erosion and scouring and gully development.
4. Based on the few maintenance records from the last two decades, rerouting the highway toward the hillside and changing its structural type from a slope-cut halfway road to a tunnel to reduce the effects of strong exogenic forces on highway are effective in the study area. A gallery tunnel mitigates the impacts of rock fall. Its construction should not cause overcut-induced slope instability, especially where water erosion and scouring are strong.

Funding The authors received financial support for this research from the Ministry of Science and Technology, Taiwan, under contracts MOST-106-2221-E-002-239-MY2 and MOST-107-2625-M-002.

References

Bar N, Barton N (2017) The *Q*-slope method for rock slope engineering. Rock Mech Rock Eng 50:3307–3322

Barton N, Lien R, Lunde J (1974) Engineering classification of rock masses for the design of tunnel support. Rock Mech 6(4):189–236

Bayer B, Simoni A, Schmidt D, Bertello L (2017) Using advanced InSAR techniques to monitor landslide deformations induced by tunneling in the northern Apennines, Italy. Eng Geol 226:20–30

Bordoni M, Persichillo MG, Meisina C, Crema S, Cavalli M, Bartelletti C, Galanti Y, Barsanti M, Giannecchini R, Avanzi GD (2018) Estimation of the susceptibility of a road network to shallow landslides with the integration of the sediment connectivity. Nat Hazard Earth Syst 18(6):1735–1758

Breschan JR, Gabriel A, Frehner M (2018) A topography-informed morphology approach for automatic identification of forest gaps critical to the release of avalanches. Remote Sens 10(3):433

Calcaterra D, Santo A (2004) The January 10, 1997 Pozzano landslide, Sorrento Peninsula, Italy. Eng Geol 75(2):181–200

Camera CAS, Apuani T, Masetti M (2014) Mechanisms of failure on terraced slopes: the Valtellina case (Northern Italy). Landslides 11(1):43–54

Chiu YC, Lee CH, Wang TT (2017) Lining crack evolution of an operational tunnel influenced by slope instability. Tunn Undergr Space Technol 65:167–178

Conforti M, Ietto F (2019) An integrated approach to investigate slope instability affecting infrastructures. Bull Eng Geol Environ 78(4): 2355–2375

Eker R, Aydın A, Hübl J (2018) Unmanned aerial vehicle (UAV)-based monitoring of a landslide: Gallenzerkogel landslide (Ybbs-Lower Austria) case study. Environ Monit Assess 190(1):28

Fallah-Zazuli M, Vafaeinejad A, Alesheykh AA, Modiri M, Aghamohammadi H (2019) Mapping landslide susceptibility in the Zagros Mountains, Iran: a comparative study of different data mining models. Earth Sci Inform 12(4):615–628

Fookes PG, Sweeney M, Manby CND, Martin RP (1985) Geological and geotechnical engineering aspects of low-cost roads in mountainous terrain. Eng Geol 21(1–2):1–152

Francioni M, Stead D, Sciarra N, Calamita F (2019) A new approach for defining slope mass rating in heterogeneous sedimentary rocks using a combined remote sensing GIS approach. Bull Eng Geol Environ 78(6):4253–4274

Giordan D, Cignetti M, Baldo M, Godone D (2017) Relationship between man-made environment and slope stability: the case of 2014 rainfall events in the terraced landscape of the Liguria region (northwestern Italy). Geomat Nat Haz Risk 8(2):1833–1852

Hartshorn K, Hovius N, Dade WB, Slingerland RL (2002) Climate-driven bedrock incision in an active mountain belt. Science 297(5589):2036–2038

Hasegawa S, Dahal RK, Yamanaka M, Bhandary NP, Yatabe R, Inagaki H (2009) Causes of large-scale landslides in the Lesser Himalaya of Central Nepal. Environ Geol 57(6):1423–1434

Hearn GJ, Shakya NM (2017) Engineering challenges for sustainable road access in the Himalayas. Q J Eng Geol Hydrogeol 50(1):69–80

Hungr O, Evans SG, Hazzard J (1999) Magnitude and frequency of rock falls and rockslides along the main transportation corridors of southwestern British Columbia. Can Geotech J 36(2):224–238

Hungr O, Leroueil S, Picarelli L (2014) The Varnes classification of landslide types, an update. Landslides 11(2):167–194

Kovács IP, Sz C, Dobre B, Fábián SÁ, Sobucki M, Varga G, Bugya T (2019) A field survey–based method to characterise landslide development: a case study at the high bluff of the Danube, south-central Hungary. Landslides 16(8):1567–1581

Lee JT (2011) A half century of lost memories: the central Cross-Island highway of Taiwan. Fourth Maintenance Office, Directorate General of Highways, MOTC, Ilan

Lee CF, Huang WK, Chang YL, Chi SY, Liao WC (2018a) Regional landslide susceptibility assessment using multi-stage remote sensing data along the coastal range highway in northeastern Taiwan. Geomorphology 300:113–127

Lee CF, Tsao TC, Huang WK, Lin SC, Yin HY (2018b) Landslide mapping and geomorphologic change based on a sky-view factor and local relief model: a case study in Hongye village, Taitung. J Chin Soil Water Conserv 49(1):27–39

Lentini V, Distefano G, Castelli F (2019) Consequence analyses induced by landslides along transport infrastructures in the Enna area (South Italy). Bull Eng Geol Environ 78(6):4123–4138

Liu TK, Hsieh S, Chen YG, Chen WS (2001) Thermo-kinematic evolution of the Taiwan oblique-collision mountain belt as revealed by zircon fission track dating. Earth Planet Sci Lett 186(1):45–56

Lo W (1992) Study of stratigraphy and geologic structures in the Hohuanshan to Tienhsiang area of Central Range, Taiwan. Doctoral dissertation, National Taiwan University

Lo W (1993) Geological map of Taiwan at scale 1:50,000 - Tayuling. Central Geological Survey, MOEA, Taipei

Mateos RM, García-Moreno I, Reichenbach P, Herrera G, Sarro R, Rius J, Aguiló R, Fiorucci F (2016) Calibration and validation of rockfall modelling at regional scale: application along a roadway in Mallorca (Spain) and organization of its management. Landslides 13(4):751–763

Meneses BM, Pereira S, Reis E (2019) Effects of different land use and land cover data on the landslide susceptibility zonation of road networks. Nat Hazards Earth Syst Sci 19(3):471–487

Milliman JD, Syvitski JPM (1992) Geomorphic/tectonic control of sediment discharge to the ocean: the importance of small mountainous rivers. J Geol 100:525–544

Palomo I (2017) Climate change impacts on ecosystem services in high mountain areas: a literature review. Mt Res Dev 37(2):179–187

Pappalardo G, Mineo S, Angrisani AC, Di Martire D, Calcaterra D (2018) Combining field data with infrared thermography and DInSAR surveys to evaluate the activity of landslides: the case study of Randazzo landslide (NE Sicily). Landslides 15(11):2173–2193

Ragmi AD, Cui P, Dhital MR, Zou Q (2016) Rock fall hazard and risk assessment along Araniko Highway, Central Nepal Himalaya. Environ Earth Sci 75(14):1112

Saha AK, Arora MK, Gupta RP, Virdi ML, Csaplovics E (2005) GIS-based route planning in landslide-prone areas. Int J Geogr Inf Sci 19(10):1149–1175

Siddique T, Masroor Alam M, Mondal MEA, Vishal V (2015) Slope mass rating and kinematic analysis of slopes along the national highway-58 near Jonk, Rishikesh, India. J Rock Mech Geotech Eng 7(5):600–606

Singh K, Kumar V (2018) Hazard assessment of landslide disaster using information value method and analytical hierarchy process in highly tectonic Chamba region in bosom of Himalaya. J Mt Sci 15(4):808–824

Strauch RL, Raymond CL, Rochefort RM, Hamlet AF, Lauver C (2015) Adapting transportation to climate change on federal lands in Washington State, U.S.A. Climate Change 130(2):185–199

TPHB (Taiwan Provincial Highway Bureau) (1960) Special issue of East and West Cross Island Highway construction. Taipei

Turowski JM, Hovius N, Hsieh ML, Lague D, Chen MC (2008) Distribution of erosion across bedrock channels. Earth Surf Process Landf 33(3):353–363

Varnes DJ (1978) Slope movement types and processes. In: Schuster RL, Krizek RJ (eds) Landslides: analysis and control, special reports 176. Transportation Research Board, National Academy of Sciences, Washington DC, pp 11–33

Vuillez C, Tonini M, Sudmeier-Rieux K, Devkota S, Derron MH, Jaboyedoff M (2018) Land use changes, landslides and roads in the Phewa watershed, Western Nepal from 1979 to 2016. Appl Geogr 94:30–40

Wang TT (2010) Characterizing crack patterns on tunnel linings associated with shear deformation induced by instability of neighboring slopes. Eng Geol 115(1–2):80–95

Wang KL, Huang ZJ (2015) Investigation and analysis of landslide and landslide dam induced by heavy rainfall with unmanned drones-an example of 74.5 K, Tai-14 express way. J Chin Inst Civil Hydraul Eng 51(3):255–261

Yang SR, Shen CW, Huang CM, Lee CT, Cheng CT, Chen CY (2012) Prediction of mountain road closure due to rainfall-induced landslides. J Perform Constr Facil 26(2):197–202

Zhang TY, Han L, Zhang H, Zhao YH, Li XA, Zhao L (2019) GIS-based landslide susceptibility mapping using hybrid integration approaches of fractal dimension with index of entropy and support vector machine. J Mt Sci 16(6):1275–1288

Zheng J, Zhao Y, Lü Q, Deng J, Pan X, Li Y (2016) A discussion on the adjustment parameters of the slope mass rating (SMR) system for rock slopes. Eng Geol 206:42–49